AT 39.3/115

Mm performance of the ATCA antennas II: effects of gravity deformations

Ravi Subrahmanyan
July 2002

The gravity deformations of the ATCA main reflector, as well as the displacements in the sub-reflector and feed, have been surveyed at a set of elevations by VMS (AT 39.3/109). In this report, I quantify these deformations and displacements and examine their effects on the antenna performance at 90 GHz. I have computed the far-field radiation pattern at each of the survey elevations and the elevation dependence of the antenna gain.

VMS photogrammetry survey

Vision Metrology Services (VMS) unit of the University of Melbourne made deformation measurements of a compact array antenna CA02 using the V-STARS photogrammetry system. The main reflector surface was defined using 398 targets; the sub-reflector location was defined with 8 targets and the feed was located with 3 targets. The antenna was set at elevations 90, 75, 60, 45, 30 and 15 degrees and was surveyed from multiple positions at each elevation setting. The survey has provided relative positions of the targets at each of the elevation settings with an accuracy of 30-50 μm (the measurements were calibrated using two invar scale bars). Assuming that the main reflector surface in the inner three rings of panels deformed the least, all of the survey data were aligned to a common frame by minimizing (in a least square sense) the deformation over these panels. A consequence of this alignment procedure is that an unknown pointing error may be introduced at every elevation and, therefore, the variation in pointing error with antenna elevation may be erroneous. The data is, nevertheless, useful for examining the gain loss and distortions in beam pattern and aperture phase, but should be used with caution for inferring the elevation dependent pointing shifts. VMS provide target positions, in an x-y-z Cartesian coordinate frame fixed w.r.t. the inner rings of panels, at each of the survey elevations.

Prior to the photogrammetry survey (done in Feb 2002), antenna holography had been used to set the panels (in Oct 1999). Holography was done using a geo-stationary satellite at an elevation of about 60 degrees. The holography is to be repeated with improved equipment. The panels of the main reflector are adjusted, based on the holography observations, to flatten the phase distribution across the aperture at the elevation of the geo-stationary satellite. Therefore, I have assumed that the antenna has an optimal flat phase aperture field distribution at 60 degrees elevation. The differences in the 3D locations of the targets at any elevation, with respect to the target locations at 60 degrees, is then interpreted as a measurement of the deformation of the optics from the optimal configuration at 60 degrees.

I might stress here that even if the antenna CA02 did not have aligned optics at the time the photogrammetry survey was done, the results of the analysis in this report will apply when the optics are aligned in the future at 60 degrees elevation, i.e., when the MR panels are set and the SR and feed are aligned for ideal optics at el=60 deg.

Gravity deformation of the main reflector

398 targets stuck to the panels define the surface of the main reflector. At el=60 degrees I assume that the main reflector has the ideal design shape. The target locations are defined by their x, y, z coordinates in a right handed Cartesian frame in which, at 60 degrees elevation, the z axis is along the symmetry axis of the main reflector and the x, y-plane is parallel to the aperture plane. Looking at the antenna aperture face on with the antenna tipped in elevation, north is up the aperture plane, south is down the plane, the EW axis is parallel to the elevation axis with east towards the right. The x-axis is positive towards south and the y-axis is positive towards east. The coordinate system is displayed in Fig. 1.

We may specify any point on the surface of the undistorted main reflector by its (x, y) coordinates on the aperture plane; the z coordinate is given by the design profile. I take the (x, y) coordinates of a target, when the antenna elevation is 60 degrees, as defining the target location. The difference (dx, dy, dz) between the (x1, y1, z1) locations of a target at any elevation and the (x0, y0, z0) coordinates of the same target at 60 degrees elevation is taken to be the displacement vector of the surface at the point (x0, y0). Differencing the target coordinates (x1, y1, z1) at any elevation δ with the target coordinates (x0, y0, z0) at elevation 60 degrees gives a vector field (dx, dy, dz) that is defined at the target locations (x0, y0). This 3-component vector field (dx, dy, dz), which is measured at specific points (x0, y0) that do not form a regular grid in 2D space, defines the deformation of the main reflector.

I have separately approximated each of the components: dx, dy & dz, of the 3-component vector field, using polynomial surfaces. The polynomials have the form

$$F(x,y) = a_{00} + a_{10}\,x + a_{01}\,y + a_{11}\,xy + a_{20}\,x^2 + a_{02}\,y^2 + a_{21}x^2y + a_{12}\,xy^2 + a_{22}\,x^2y^2 + \dots,$$

$$F(x,y) = \sum a_{mn}\,x^m\,y^n,$$

where m & n separately take on all integral values from 0 to k and k is the degree of the polynomial surface.

A k^{th} degree polynomial surface is defined using $(k+1)^2$ coefficients. I have fitted k=5 degree polynomial surfaces. With 398 target points, solving for the 36 coefficients is an over determined problem and the coefficients have been solved for as a best approximation in a least square sense using singular value decomposition. The r.m.s. of

the fit surface and the r.m.s. of the residuals to the fit, for the dx, dy and dz deformation components and at elevations 90, 75, 45, 30 & 15 degrees, are summarized in Table 1. The VMS report gives the survey accuracy to be in the range 35-50 μm and the errors in the target displacements (difference measurements) would be expected to be about √2 larger. The r.m.s. of the residuals to the fits (see Table 1) is in the range 50-70 μm and this is consistent with the survey accuracy. Increasing the order of the polynomial surface reduces the r.m.s. of the residuals only marginally; therefore, I have limited the order to k=5 and deemed these polynomials as sufficient to describe the surface deformation.

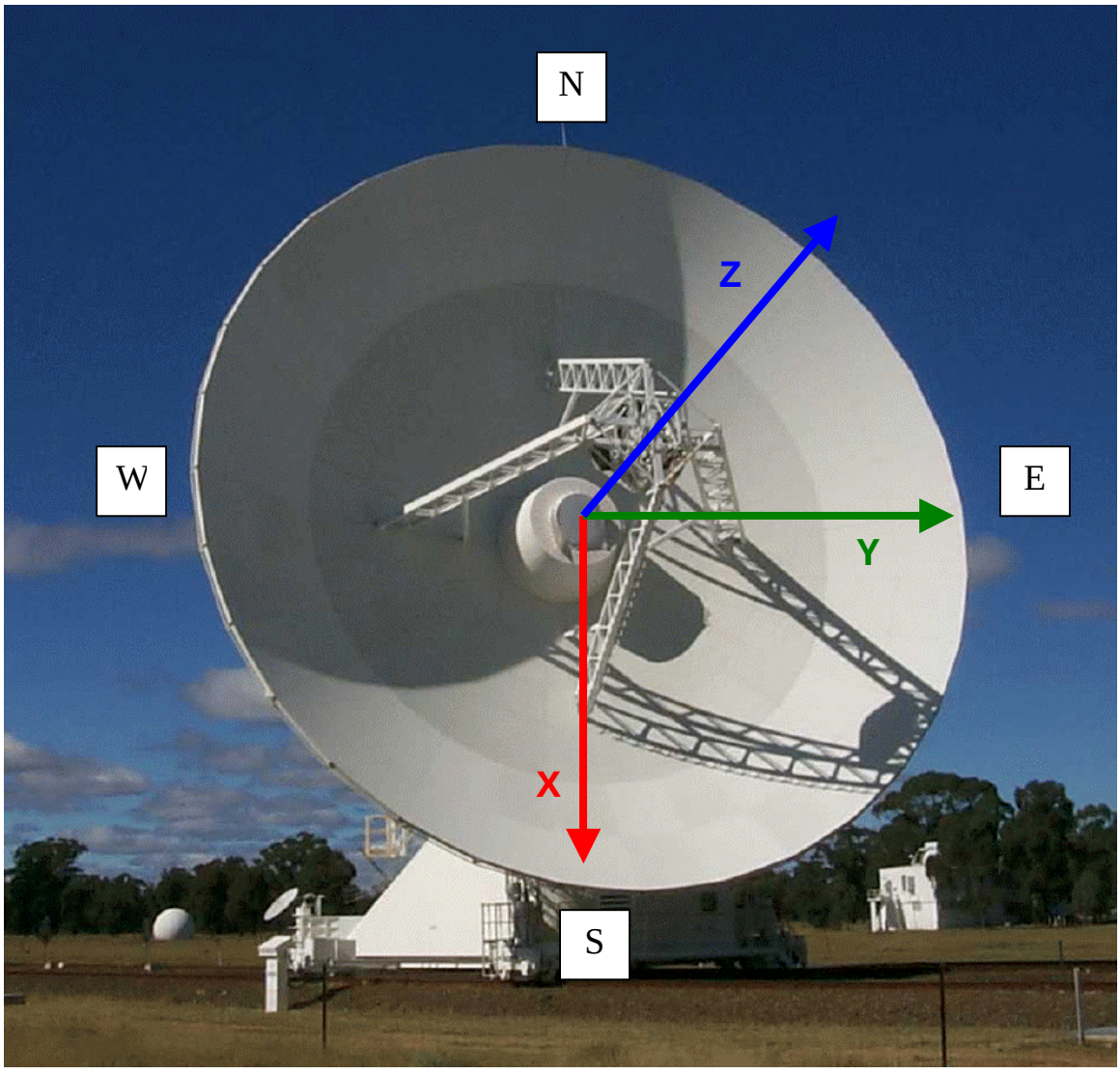

Figure 1: The definition of the coordinate system.

The r.m.s. displacement of the surface, at the target locations, is about 400 μm at 90 degrees elevation and 490 μm at 15 degrees elevation. The dy component of the

displacement, parallel to the elevation axis and perpendicular to the gravity vector, is understandably the smallest.

Elevation	**dx**		**dy**		**dz**	
(degrees)	poly fit	residuals	poly fit	residuals	poly fit	residuals
90	340	50	116	54	166	58
75	189	58	113	54	109	57
45	149	51	127	45	158	56
30	259	49	189	46	299	57
15	304	56	205	52	323	71

Table 1: Polynomial surface fits to the x, y, z components of the surface deformations. The r.m.s. of the polynomial surfaces at the target positions, as well as the r.m.s. of the residuals, are tabulated. The r.m.s. values are in μm.

I show images of the deformation in Fig. 2, where the component of the displacement vectors perpendicular to the local surface are displayed. The same deformation is shown using profile plots in Fig. 3. The antenna main reflector is being viewed face on in these images. It is seen here that at low elevations, the outer panels in the north half of the antenna deform forwards where as in the south part of the main reflector the structure is displaced backwards. This is the dominant first order deformation and is as expected due to gravity. This cosine(azimuth) type deformation will give rise to a large coma lobe on the south side of the main lobe. There is also higher order deformation in the main reflector and that is clearly seen in the plots made at the highest and lowest elevations. These are probably related to the radial ribs of the backup structure: the gravity vector is in the x-z plane and the x-component of this force may be causing the higher order deformations in the axially symmetric backup structure. The higher order MR deformation will result in higher order asymmetries in the antenna beam pattern. In this context, I wonder if an alt-azimuth antenna ought to have backup ribs oriented in the x-z plane instead of being radial.

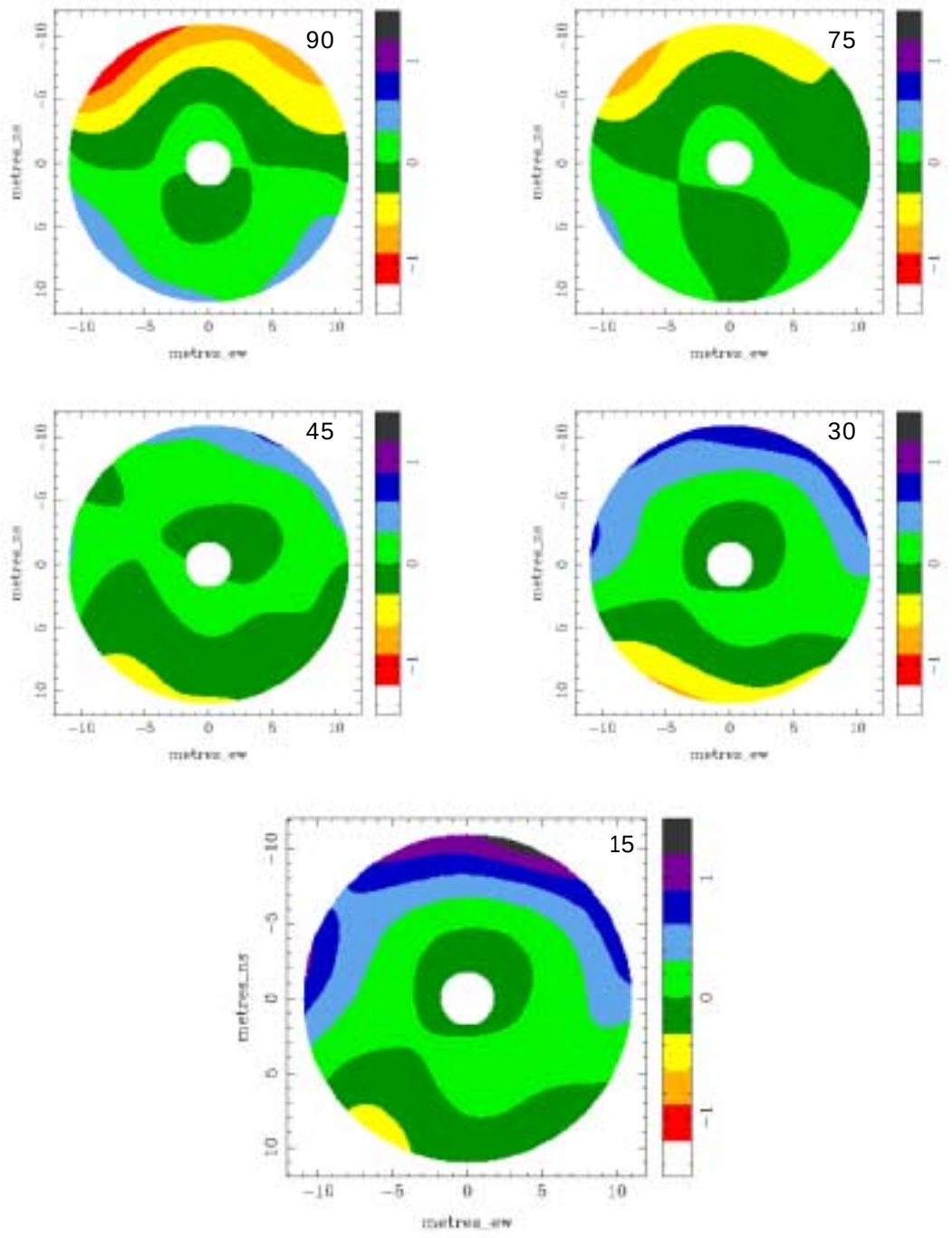

Figure 2: The deformation in the main reflector surface at different antenna elevations. The component of the surface deformation vector perpendicular to the surface is shown here. The elevations are marked in the upper right corner of the panels. The wedges that colour code the displacement scale are marked in mm. The figures show the antenna face on, with the lightning rod at the top of the figures.

(a) Elevation = 90

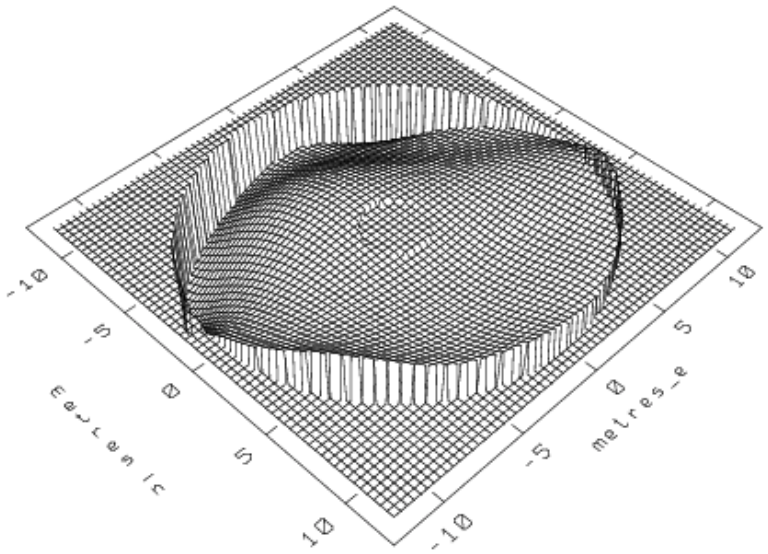

(b) Elevation = 75

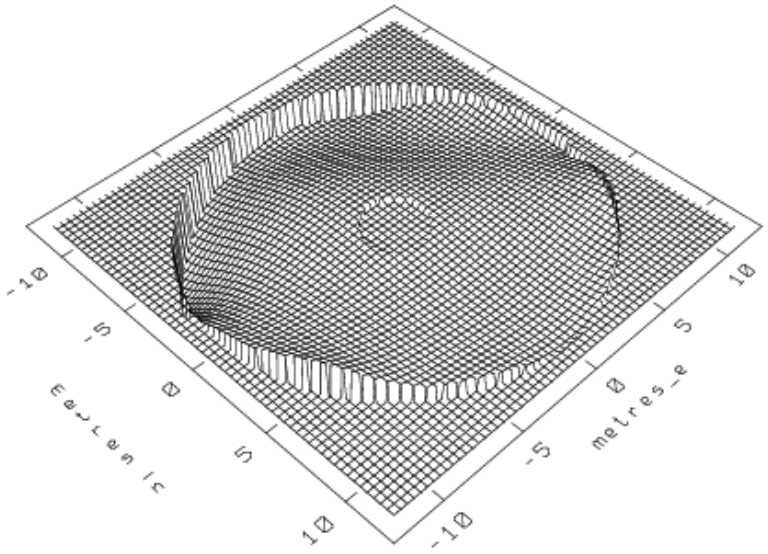

(c) Elevation = 45

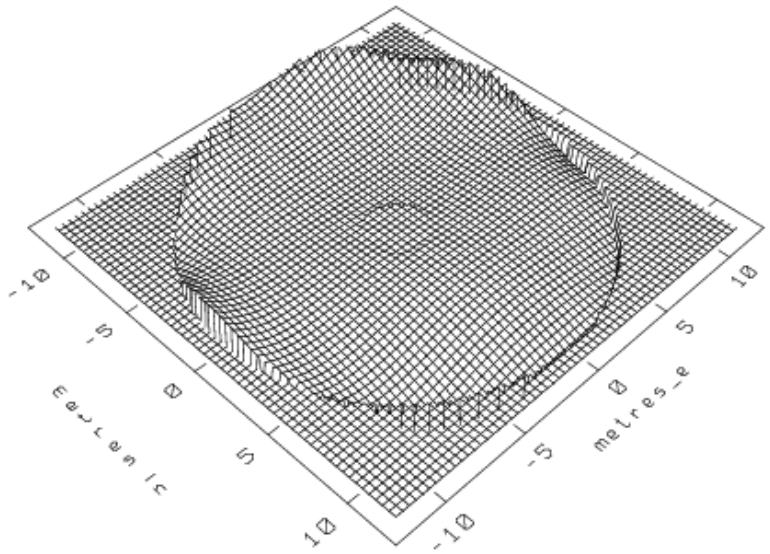

(d) Elevation = 30

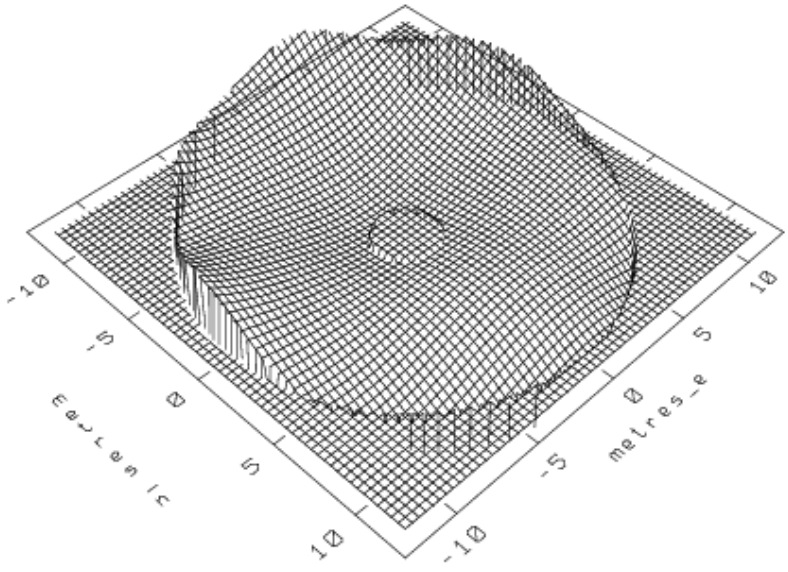

(e) Elevation = 15

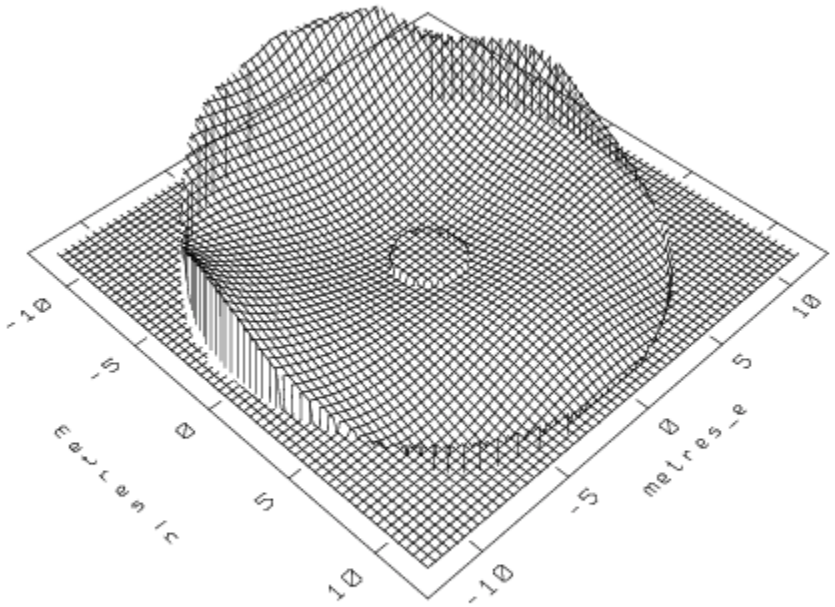

Figure 3: Profile plots of the elevation dependent deformation of the main reflector surface. The z-axis is the component of the deformation vector normal to the surface. The x-y plane represents the antenna face; the plots show the dish viewed face on with the northern end of the antenna face (the end with the lightning rod) at the top of the plot.

Gravity deformation of the sub-reflector

The sub-reflectors in the compact array antennas are (rigidly) connected to a rectangular box frame and this frame is suspended from the quadrupod structure by 16 wire ropes under tension. During the photogrammetry survey of the compact array antenna ca02, VMS also placed targets on the quadrupod structure as well as on the top surface of the sub-reflector and on the box frame. Unfortunately, all these targets were not visible in all the survey elevations. For each elevation position of the antenna, i.e., at 15, 30, 45, 60, 75 and 90 degrees elevation, VMS provide the x, y and z locations of a subset of these targets. The target locations are specified at any elevation in the Cartesian reference frame determined (for that elevation) by the inner rings of panels on the main reflector.

I first examined the gravity-induced displacement of the SR. I consider the SR and the box frame to which it is connected as a single rigid system. This system is allowed three

translation and three rotational degrees of freedom. Taking the position and orientation of the SR at el=60 degrees as reference, the displacement of the SR at 15, 30, 45, 75 and 90 degrees is described using a total of 6×5=30 parameters. I have used all the target position data provided by VMS and for each pair of elevations I have computed the displacement vectors for every target that is surveyed at both the elevations. This results in 174 target pairs. The 30 displacement parameters were fitted, via non-linear optimization, to the displacement vectors of the 174 target pairs. VMS estimate errors for every target position and these errors were used as weights for the optimization. The fit residuals had a variance 3.6 times worse than expected indicating that either the error estimates provided by VMS were an underestimate and/or that the SR+box is not a rigid structure. The SR displacements and rotations (w.r.t. ideal optics at 60 degrees elevation) are given in Table 2. I show the displacements and tilts of the SR, projected on the x-z plane, in Fig. 4.

It may be noted here that a rotation of 0.02 degrees corresponds to a displacement of 0.5 mm at the edge of the SR. The rotations measured about the x and z-axes are tiny; however, there appears to be a systematic rotation about the y (elevation) axis. As the antenna tips in elevation, gravity rotates the southern end of the SR away from the MR. The total rotation of 0.03 degrees between 90 and 15 degrees corresponds to linear movements of the southern and northern tips of the SR through 0.7 mm.

There is an indication for a systematic z-axis movement of the SR; as the antenna tips in elevation from 75 to 15 degrees, the SR moves away from the MR and the total travel is 0.35 mm over this elevation range. The measured x and y axis displacements are within ±0.4 mm and do not appear to be systematic. I believe that this is because the target positions at the different elevations are not tied to a single coordinate frame but are tied to the inner rings of main reflector panels; the pseudo-random x-y displacements in table 2 may be due to deformations in the inner parts of the main reflector.

The displacement of the SR, w.r.t. the MR, is really all that we need compute for the purpose of evaluating the antenna performance.

I have fitted for the displacement and rotation of the top of the quadrupod structure w.r.t. the MR. For this exercise, I have used only those targets that are on the quadrupod and at the height of the SR+frame. In this case, there are 314 target pairs to constrain the solutions. The residuals to the fit have a variance 3 times more than expected. The solutions for the displacement of the top of the quadrupod, w.r.t. the MR, is in Table 3. The displacement is displayed in Fig. 5.

In the frame of the MR, the top of the quadrupod has x and y coordinate displacements that are within ±0.4 mm and do not vary systematically with elevation. There is a systematic z-axis movement of the top of the quadrupod, which travels through 0.45 mm towards the MR as the antenna tips from 90 to 15 degrees in elevation. It may be noted here that as the antenna tips, the SR has a 0.25 mm z-axis movement away from the MR while the quadrupod has a 0.45 mm z-axis movement towards the MR; these together imply that the SR moves through about 0.7 mm w.r.t. the top of the quadrupod. There is a

small systematic rotation of the top of the quadrupod through 0.002 degrees about the x-axis as the antenna tips in elevation. There is also a more significant rotation through 0.02 degrees about the y (elevation) axis. This rotation is in the same sense as the rotation in the SR and implies that most of the rotation seen in the SR is due to gravity deformation of the quadrupod structure.

The solutions for the displacements of the SR and for the top of the quadrupod were independently obtained from completely different sets of targets. I have differenced these two solutions to examine the displacement of the SR w.r.t. the top of the quadrupod. These differential solutions are given in Table 4 and the corresponding SR displacement, w.r.t. the quadrupod, is displayed in Fig. 6.

The derived differential displacement of the SR, w.r.t. the top of the quadrupod, is dominantly an axial movement. As the antenna tips, the SR moves upwards and away from the MR, the total travel is estimated to be 0.7 mm from 90 to 15 degrees elevation. There is also a small displacement of the SR towards south through 0.3 mm as the antenna tips. The tilts in the SR, w.r.t. the quadrupod structure, are small and less than 0.01 degrees.

It may be noted here that the ATCA antennas have an LVDT attached to the top of the quadrupod structure that measures the axial position of the SR w.r.t. the top of the quadrupod. As the antenna tips in elevation, the LVDTs show that the SR moves axially and towards the top of the quadrupod; the total travel has been measured to be about 0.7 mm. This confirmation gives confidence in the derivation of the SR movement from the photogrammetry. It is because the trend and values in table 4 are as expected that I have confidence in the solutions given in table 2.

The measured lateral displacements and tilts in the SR are indeed tiny. We see x-y plane displacements within ±0.4 mm and tilts within ±0.02 degrees. The effects of tilts and displacements in the SR, for 3 mm operation, were analyzed in AT 39.3/113. It is seen from that analysis that the measured tilts and displacements of the SR would not be expected to result in gain loss more than 1%.

The displacement in the SR that is of most concern is the axial movement because, as seen from the results in AT 39.3/113, for the same magnitude of displacement an axial movement results in a greater gain loss as compared to a lateral shift. The measured axial movement of the SR, w.r.t. the MR, is about 0.3 mm (Table 2). It is interesting that as the antenna tips in elevation, the solutions show that the top of the quadrupod moves down towards the MR (by 0.45 mm) while the SR moves up towards the top of the quadrupod (by 0.7 mm). The quadropod structural deformation partially compensates for the SR movement w.r.t. the quadropod. Alternately, the sag in the ropes holding the SR overcompensates for the axial gravity displacement of the top of the quadrupod structure. These two opposite movements limit the net axial SR movement to about 0.3 mm. This net movement is not expected to result in a gain loss much more than 1%.

	X displacement	Y displacement	Z displacement	X rotation	Y rotation	Z rotation
15	0.33	-0.08	0.31	-0.005	-0.009	0.005
30	0.37	-0.09	0.27	-0.006	-0.006	0.005
45	0.12	-0.08	0.01	-0.006	-0.002	0.008
75	0.23	0.11	-0.04	0.004	0.013	-0.003
90	0.25	-0.06	0.06	-0.002	0.019	0.007

Table 2: The x,y,z coordinate displacements (in mm) of the SR, and the rotation (in degrees) of the SR about the x, y and z axes, when the antenna is moved in elevation from 60 degrees to the elevation specified in the first column.

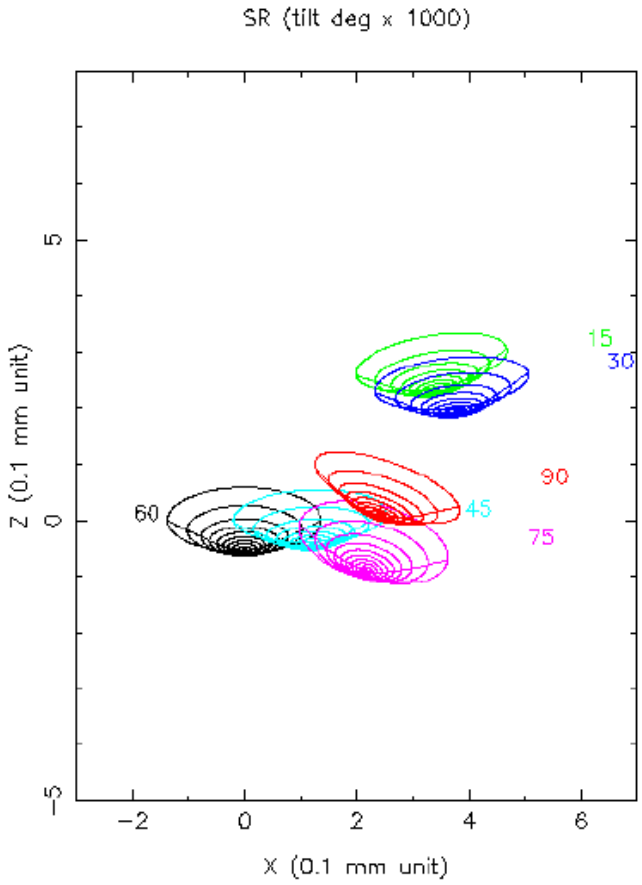

Figure 4: The displacement and tilt of the SR, w.r.t. the MR, at different elevations. The displacements are viewed projected on the x-z plane. The SR is shown nominally tilted by 25 degrees towards the viewer. The axes are in units of 0.1 mm. The tilts are magnified by factor 1000 in angle.

	X displacement	Y displacement	Z displacement	X rotation	Y rotation	Z rotation
15	0.15	-0.08	-0.31	0.000	-0.007	0.001
30	0.24	-0.11	-0.14	0.001	-0.003	0.001
45	0.10	-0.08	-0.13	0.001	-0.003	0.002
75	0.30	-0.02	0.05	0.002	0.007	0.003
90	0.33	-0.14	0.13	0.002	0.014	0.006

Table 3: The x,y,z coordinate displacements (in mm) of the top of the quadrupod, and the rotation (in degrees) of this part about the x, y and z axes, when the antenna is moved in elevation from 60 degrees to the elevation specified in the first column.

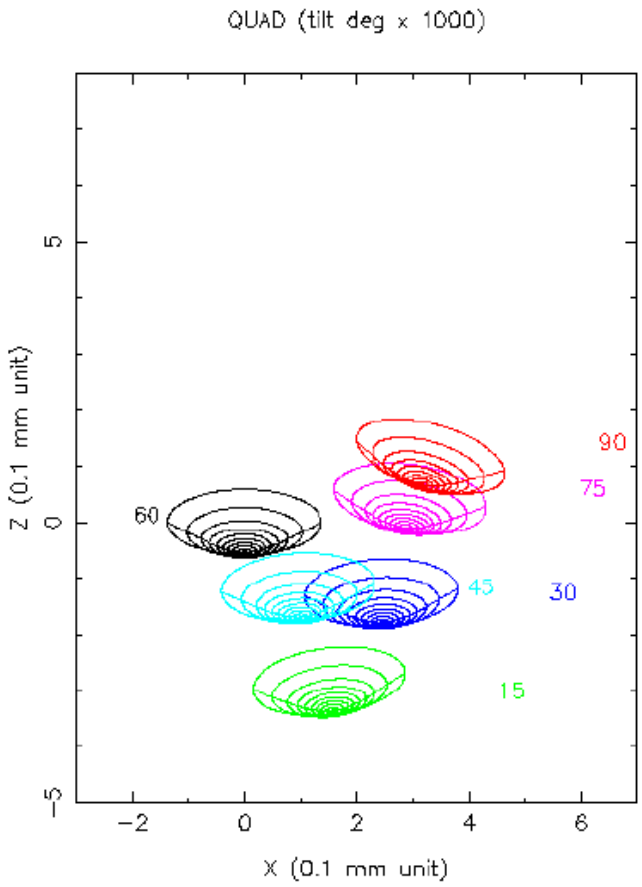

Figure 5: The displacement and tilt of the SR if it were rigidly fixed to the top of the quadrupod structure. The displacements are viewed projected on the x-z plane. The SR is shown nominally tilted by 25 degrees towards the viewer. The axes are in units of 0.1 mm. The tilts are magnified by factor 1000 in angle.

	X displacement	Y displacement	Z displacement	X rotation	Y rotation	Z rotation
15	0.18	0.01	0.62	-0.006	-0.002	0.004
30	0.13	0.02	0.41	-0.007	-0.003	0.005
45	0.02	0.00	0.14	-0.007	0.001	0.006
75	-0.07	0.13	-0.09	0.002	0.006	-0.006
90	-0.08	0.08	-0.06	-0.004	0.005	0.001

Table 4: The x,y,z coordinate displacements (in mm) of the SR w.r.t. the quadrupod, and the rotation (in degrees) of the SR about the x, y and z axes, when the antenna is moved in elevation from 60 degrees to the elevation specified in the first column.

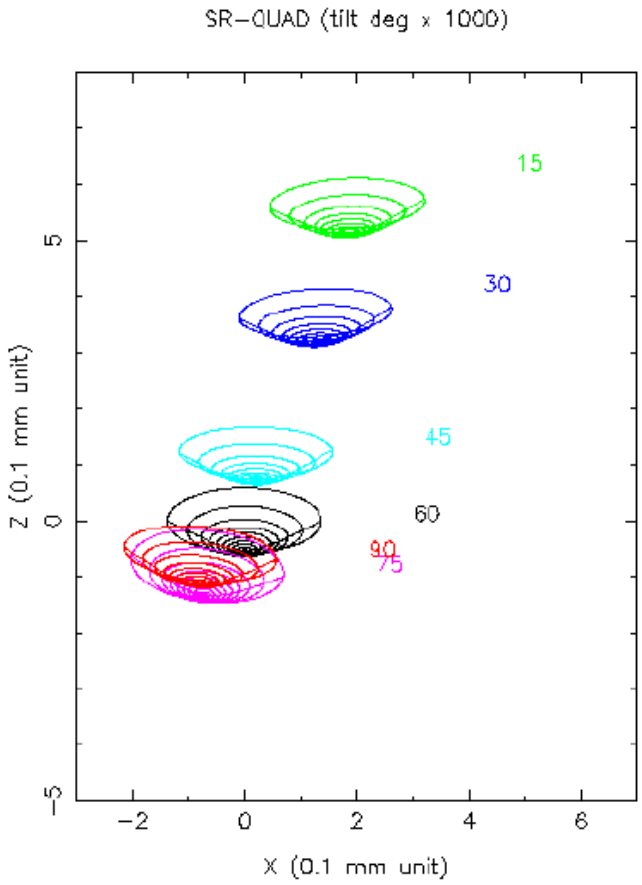

Figure 6: The displacement and tilt of the SR w.r.t. the top of the quadrupod structure. The displacements are viewed projected on the x-z plane. The SR is shown nominally tilted by 25 degrees towards the viewer. The axes are in units of 0.1 mm. The tilts are magnified by factor 1000 in angle.

Gravity displacement of the feed

The VMS survey had three targets on a frame that was fixed to the turret in which the feeds are located. The locations of these targets were also determined, at each survey elevation, in the coordinate frame fixed to the inner rings of main reflector panels. In Fig.7 I show the mean x, y & z coordinate displacements of the three targets versus the antenna elevation. The displacements are also listed in Table 5. The differences in the individual target displacements from the mean were consistent with the expected errors: the displacement measurements had standard deviations of 54, 68 and 87 μm. The most significant displacement of the feed (in the reference frame) is along the x-axis where the measurements show a systematic movement through 2.3 mm towards south as the antenna tips in elevation. The x and z axis displacements are both within ±0.5 mm.

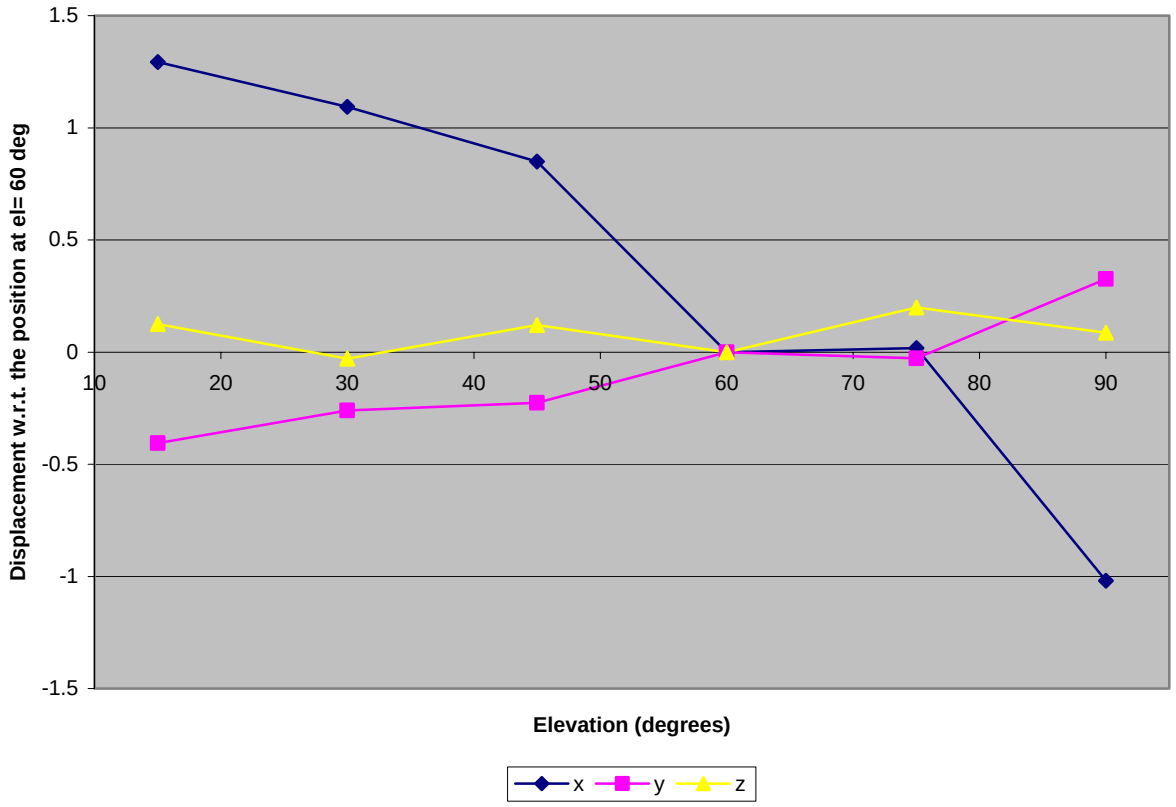

Figure 7: The mean displacement of the feed in the x, y & z directions versus the antenna elevation. The displacement is in mm units. The displacement is measured w.r.t. a coordinate frame tied to the inner rings of main reflector panels.

Elevation (degrees)	x	y	z
15	1.29	-0.41	0.12
30	1.09	-0.26	-0.03
45	0.85	-0.23	0.12
60	0	0	0
75	0.02	-0.03	0.20
90	-1.02	0.33	0.09

Table 5: The displacement of the feed (in mm) along the x, y & z axes. The first column gives the antenna elevation. The feed is assumed to be at its ideal location at 60 degrees elevation.

The measured lateral displacements of order ±1 mm are of little consequence to the antenna gain; however, a 2.3 mm displacement will result in a pointing shift of 8.2 arcsec over the 15-90 degree elevation range. To first order, any systematic pointing shift would be automatically accounted for in the pointing model.

A second aspect to note is that the measured feed displacement along the x-axis does not imply that the turret sags due to gravity. It may be that the gravity deformation of the inner rings of main reflector panels alters the coordinate frame, in which the feed position is being measured, systematically with elevation.

A GO ray-tracing analysis of the gravity deformations:

In the sections above I have characterized the gravity deformation/displacements of the MR, SR and feed. These three components together define the ATCA antenna optics. All the deformations/displacements at a fixed elevation are described in a common frame tied to the inner rings of panels. In this section, I analyze their combined effect on the antenna performance at mm wavelengths.

For this purpose, I have used a geometric optics approximation. The 3D ray-tracing routines I developed in AT 39.3/113 have been modified to

1. Allow for deformations of the main reflector that are described by three 2D polynomial functions, and
2. Allow for a 6-parameter SR displacement (x, y, z coordinate displacements and rotations about the x, y & z axes).

The antenna is assumed to have ideal optics at an elevation of 60 degrees. At each of the other survey elevations (15, 30, 45, 75 & 90 degrees) I have

1. Deformed the main reflector using the coefficients that were derived by fitting to the MR targets,
2. Displaced and rotated the SR using the parameters computed for that elevation, and
3. Displaced the feed.

All computations were made at a frequency of 90 GHz. Ray tracing was used to derive the aperture illumination for the gravity-deformed optics and the far-field radiation pattern of the antenna was computed. The relative gains at the different elevations are listed in Table 6 and a plot of the gain variation with antenna elevation is in Fig. 8. The gains are normalized to the value at el=60 deg. In the reference frame defined by the central rings of panels, the offset in the antenna pointing from the z-axis has been determined and these values are also listed in Table 6.

Antenna Elevation (degrees)	Power gain (relative to the gain at 60 deg.)	Pointing offset (arcsec) X	Y
15	0.69	4.9	–2.3
30	0.77	4.8	–3.3
45	0.95	2.1	–3.4
60	1.0	0.0	0.0
75	0.94	-11.5	–2.0
90	0.93	-14.9	–3.4

Table 6: Antenna gain and pointing offsets at different elevations. The gain loss values are for 90 GHz operation; the pointing offsets ought to be frequency independent.

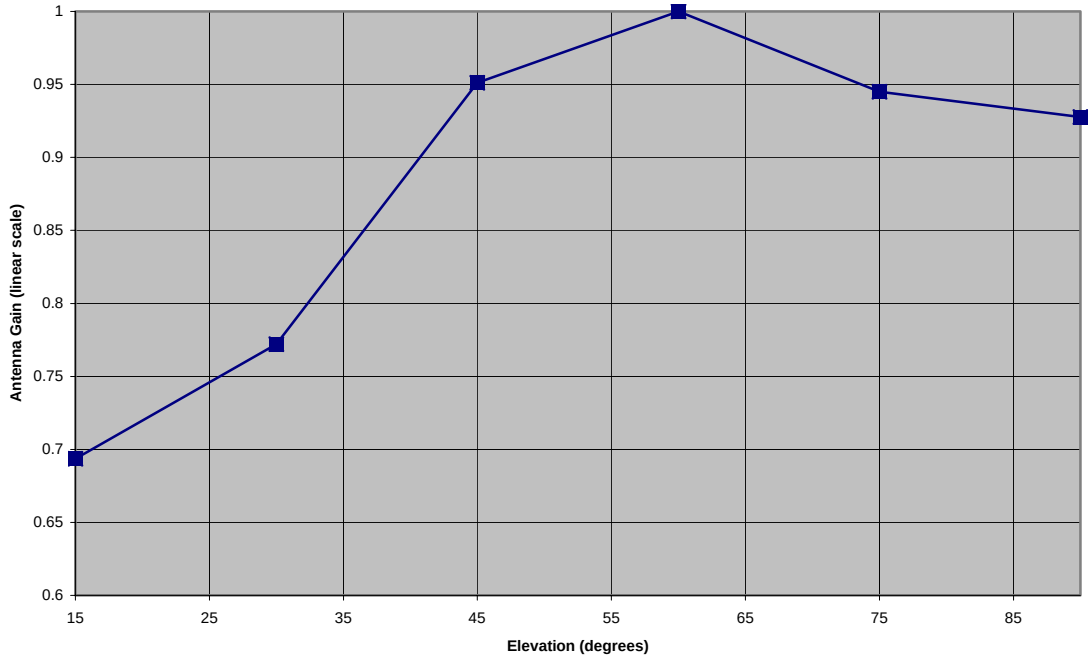

Figure 8: Antenna power gain at 90 GHz, normalized to the value at 60 degrees elevation, versus the antenna elevation.

The gravity vector acts in the x-z plane and we expect the displacements and MR deformations to primarily cause coma lobes along the NS line. The higher order MR

deformations, particularly at high elevations, would be expected to result in higher order beam distortions. In Fig. 9, I have displayed NS slices across the 2D beam patterns that have been computed at the different survey elevations. At low elevations, a coma lobe appears to the south of the main lobe. At high elevations no coma lobe appears along the NS line; however, the depth of the first nulls is reduced and this is indicative of a change in the focal length of the MR.

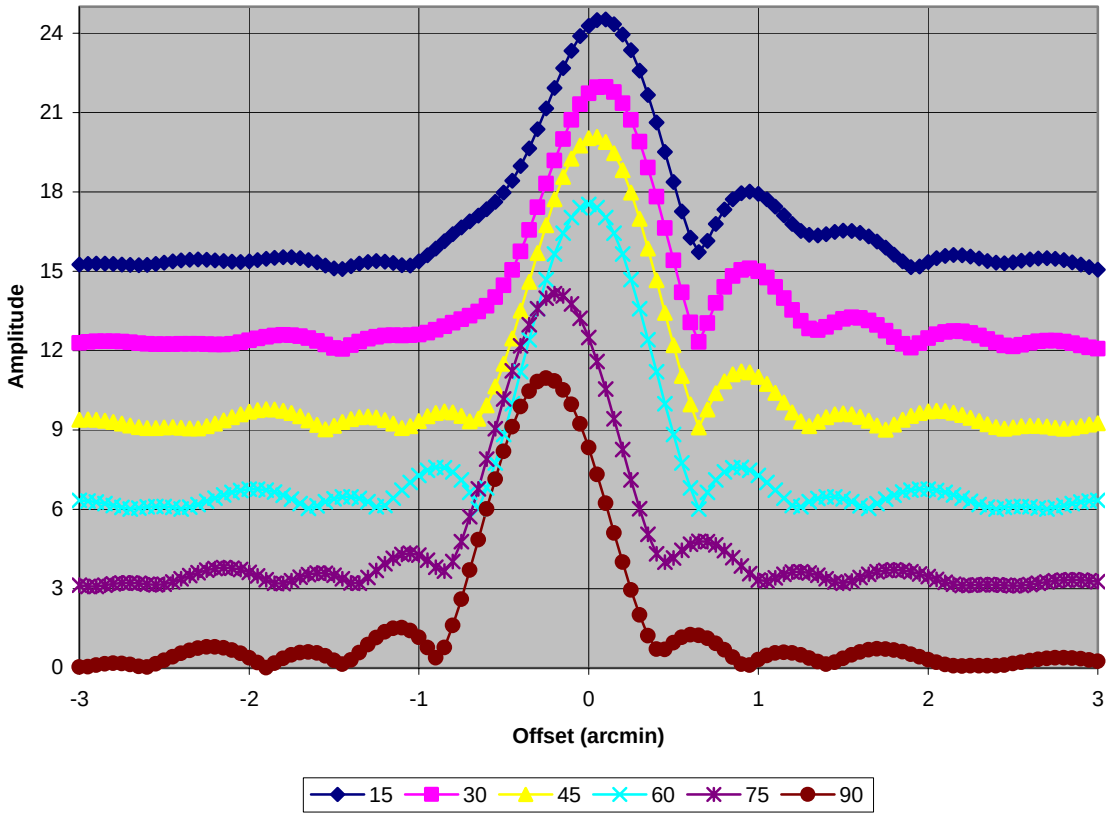

Figure 9: N-S slices across the 90 GHz beam patterns. Positive offsets are towards south; the coma lobe at low elevations appears to the south of the main lobe. Slice profiles at different elevations have been vertically offset for clarity.

The 2D beam patterns at each of the survey elevations are shown in Fig. 10 as contour plots with gray-scales overlaid. These are images of the amplitudes of the voltage radiation pattern and not the power pattern.

At low elevations (below 60 deg.) the first order gravity deformation dominates and a large coma lobe appears to the south of the main lobe. For the ideal optics case the first sidelobe of the power pattern is expected at about 2% as compared to the main lobe. At el=15 deg., the coma lobe is at 12%; at el=30 deg., the coma lobe is 11% of the main lobe and at el=45 deg., the coma lobe is at 6% level. At high elevations (above 60 deg.) the higher-order azimuthal deformations of the main reflector result in higher order beam distortions. The dominant sidelobes that appear to the NE and NW of the main lobe have peak powers 5% and 7% at elevations of 75 and 90 degrees respectively.

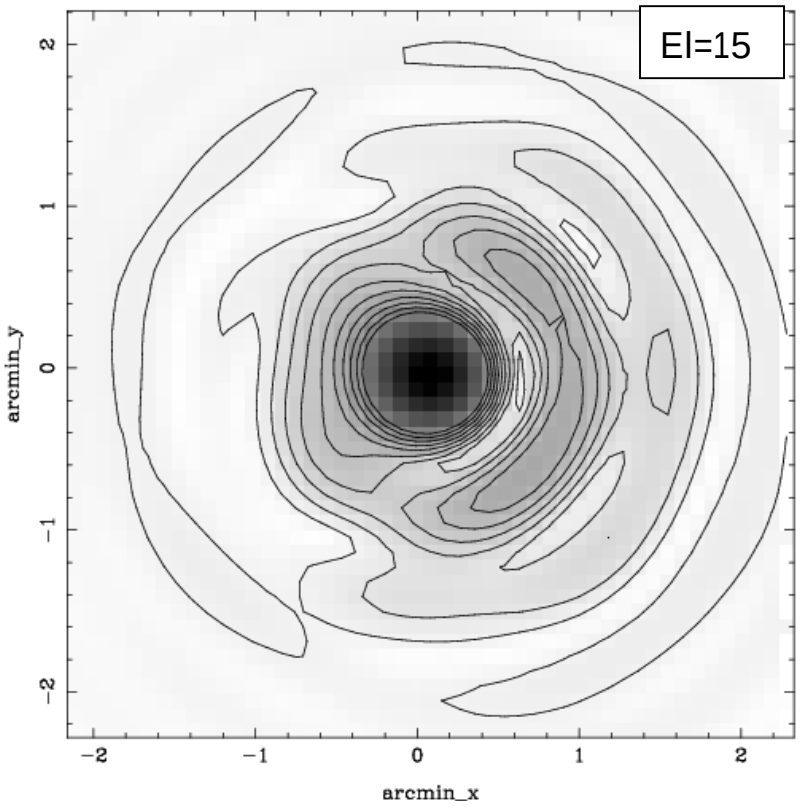
El=15
arcmin_y
arcmin_x
2
1
0
−1
−2
−2
−1
0
1
2

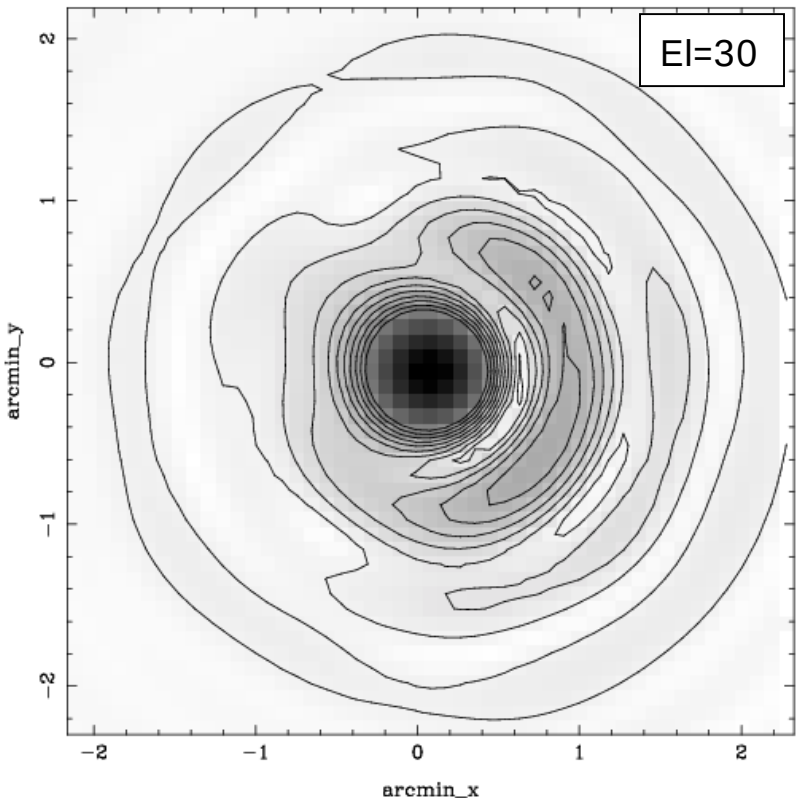
El=30
arcmin_y
arcmin_x
2
1
0
−1
−2
−2
−1
0
1
2

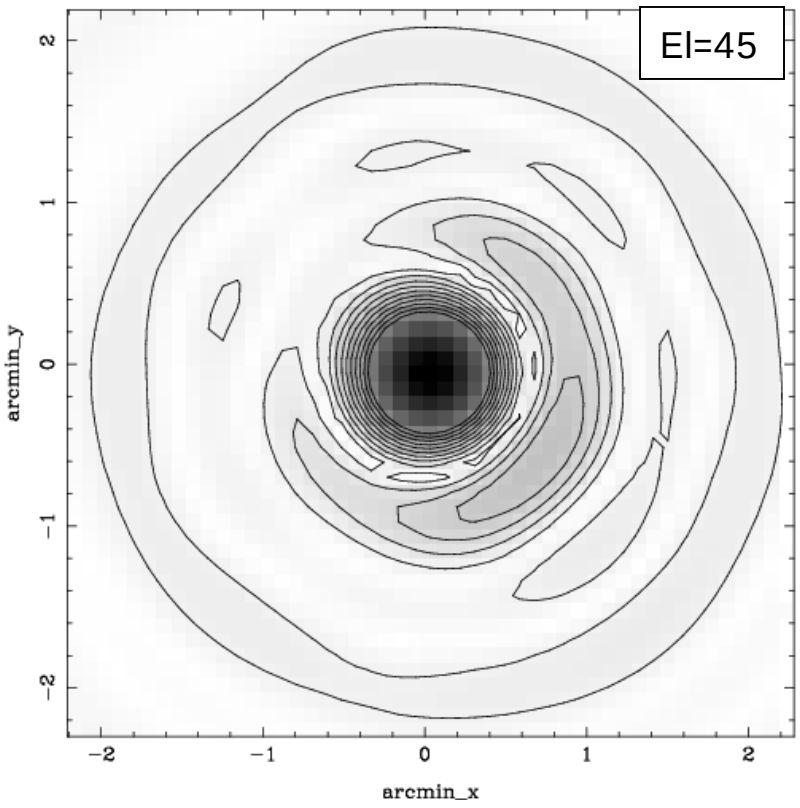
El=45
arcmin_y
arcmin_x
2
1
0
−1
−2
−2
−1
0
1
2

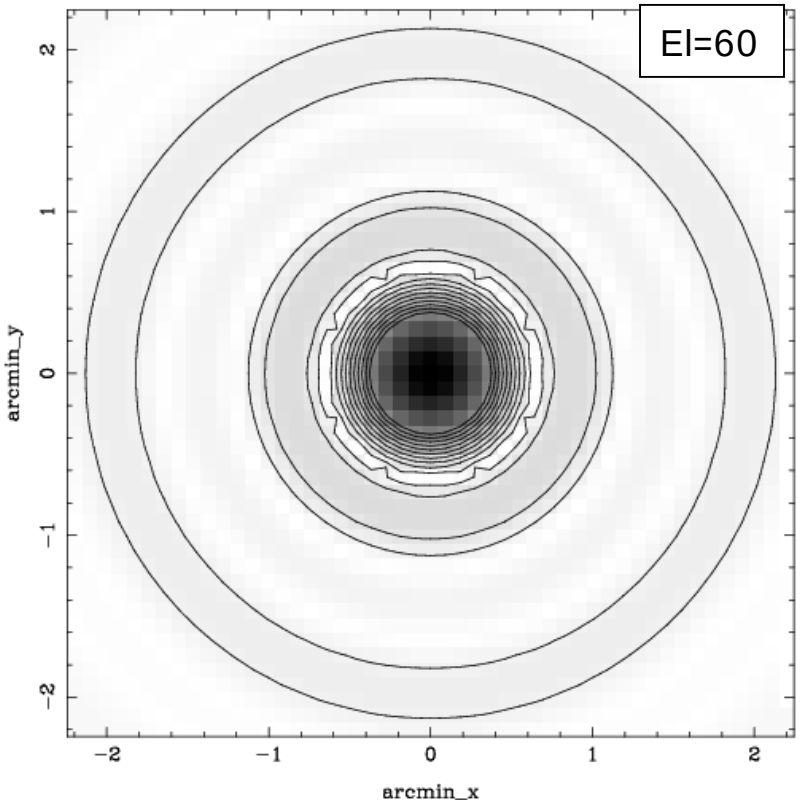
El=60
arcmin_y
arcmin_x
2
1
0
−1
−2
−2
−1
0
1
2

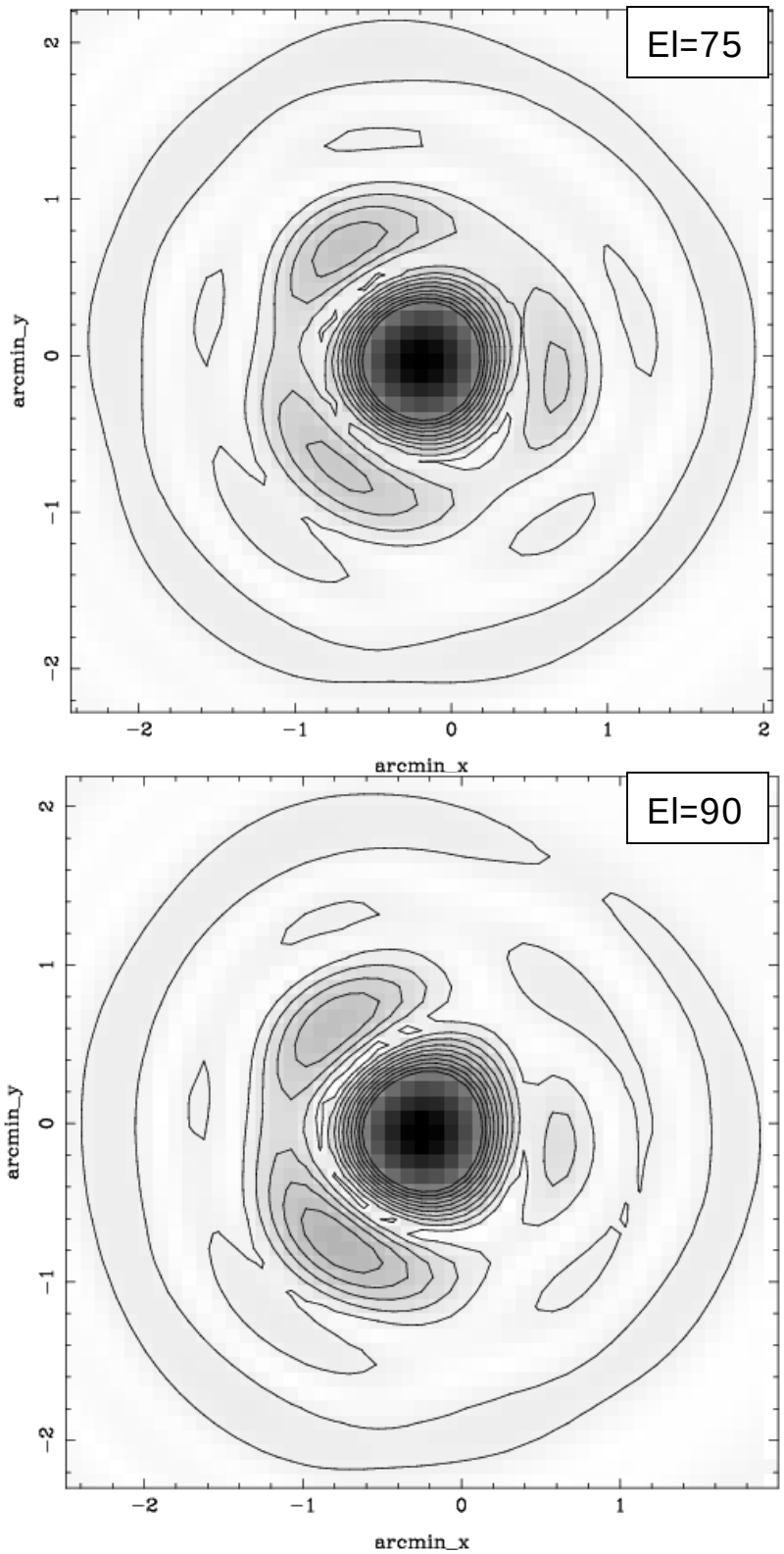

Figure 10: Computed beam patterns, at 90 GHz, at the elevations where the photogrammetric survey were made. The amplitude of the voltage pattern is shown. Contours are shown at 5% intervals; the maximum contour is at 50% of the peak. North is to the left of the panels.

The antenna pointing error is usually determined by nominally pointing the array to an unresolved source, making a positive and a negative angular offset in elevation and in azimuth (or at ±45 deg. to the vertical), and examining the drops in visibility amplitude. The magnitude of the offset is calculated so that the visibility amplitude would drop by 50% if there were no pointing error. This method relies on the symmetry of the beam; if the beam is skewed, the method will fail to give a good solution. The highest contour shown in the beam pattern images is at 50% of the peak. This contour is at 25% power level and is clearly not circular at some elevations.

At 90 GHz, the ideal beam power pattern has a FWHM of 33 arcsec (as derived from the el=60 deg. beam pattern). At each of the survey elevations, I have examined the 70% contour level (half power beam) and the location of the beam peak w.r.t. this contour. Over the elevation range of 15-90 degrees, the HPW of the beam is within the range 32.0-33.3 arcsec. The ellipticity of the beam is greatest at the lowest elevation where the ratio of the major to minor axes of the half power contour is 1.03. The skew in the beam also increases as the antenna tips in elevation: the peak of the beam is offset 0.8 arcsec from the center of the half-power ellipse at el=30 deg., the offset is 1 arcsec at el=15 degrees.

Summary:

1. The gravity deformation of the MR is dominated by a cosine(azimuth) form surface displacement at low elevations. At high elevations, deformation corresponding to higher order terms is also apparent. The surface deviation, measured normal to the surface, has r.m.s. values of 0.4 and 0.5 mm at elevations 90 and 15 degrees respectively. The surface deviation takes values in the range –1 to +0.5 mm at el=90 and –0.5 to +1.5 mm at el=15 degrees. At mm wavelengths, this MR deformation appears to me to be the dominant cause for elevation dependent gain loss and beam distortions.

2. As the antenna tips in elevation from 90 to 15 degrees, the SR moves axially through 0.3 mm away from the MR. Additionally, in a frame fixed to the inner rings of main reflector panels, the SR rotates about the elevation axis through 0.03 degrees. This rotation moves the south end of the SR away from the MR and the north end towards the MR; the rotation corresponds to movements of 0.7 mm at the north and south ends. These movements are not expected to cause a gain loss much more than 1%.

3. The feed moves 2.3 mm south as the antenna tips in elevation; this displacement is in the coordinate frame fixed to the inner rings of MR panels. The gain loss due to this measured displacement is expected to be much less than 1%.

4. GO analysis of the gravity deformed antenna yields a gain loss factor of 0.7 at 15 degrees elevation and a loss factor of 0.93 at 90 degrees elevation. These loss factors for the antenna power gain are with respect to an undistorted antenna at 60 degrees elevation.

5. The gravity deformation of the antenna is expected to result in a significant coma lobe at low elevations. At el=30 degrees, the coma lobe in the antenna power pattern is expected to be 11% of the main lobe. At high elevations, the beam pattern is expected to have higher order distortions and the computed power patterns show 5-7% sidelobes to the NE and NW of the main lobe.

6. Above the half-power level, the beam ellipticity and skew are at the arcsec level. However, at lower power levels the beam is increasingly skewed; therefore, the algorithm for solving for the pointing error needs to be iterative if the initial error is significant. I would not expect the pointing to be compromised by the beam shape and I would expect an iterative algorithm to converge to within 1 arcsec (provided the asymmetry in the beam is the dominant limiting factor).